

STRIPE-LIKE INHOMOGENEITIES, SPECTROSCOPIES, PAIRING, AND COHERENCE IN THE HIGH- T_c CUPRATES

J. ASHKENAZI

Physics Department, University of Miami, P.O. Box 248046, Coral Gables, FL 33124, U.S.A.

Abstract—It is found that the carriers of the high- T_c cuprates are polaron-like “stripons” carrying charge and located in stripe-like inhomogeneities, “quasi-electrons” carrying charge and spin, and “svivons” carrying spin and lattice distortion. This is shown to result in the observed anomalous spectroscopic properties of the cuprates. The AF/stripe-like inhomogeneities result from the Bose condensation of the svivon field, and the speed of their dynamics is determined by the width of the double-svicon neutron-resonance peak. Pairing results from transitions between pair states of stripons and quasi-electrons through the exchange of svivons. The obtained pairing symmetry is of the $d_{x^2-y^2}$ type; however, sign reversal through the charged stripes results in features not characteristic of this symmetry. The phase diagram is determined by a pairing and a coherence line, associated with a Mott transition, and the pseudogap state corresponds to incoherent pairing.

I. INTRODUCTION

The existence of stripe-like inhomogeneities in the high- T_c cuprates has been predicted theoretically quite early [1]. A wealth of experimental data support the existence of such inhomogeneities, at least dynamically, in the superconducting (SC) and the pseudogap states. The underlying striped structure is characterized by narrow charged stripes forming antiphase domain walls between wider antiferromagnetic (AF) stripes [2].

Experimental observations in the cuprates have been also pointing to the presence of both itinerant and almost localized (or polaron-like) carriers in the cuprates. First-principles calculations [3] support an approach based on the existence of both large- U and small- U orbitals in the vicinity of the Fermi level (E_F), and the applicability of a t - t' - J model for the CuO_2 planes.

A small- U electron in band ν , spin σ (which is assigned a number ± 1), and wave vector \mathbf{k} is created by $c_{\nu\sigma}^\dagger(\mathbf{k})$. The large- U electrons in the CuO_2 planes are approached by the “slave-fermion” method [4]. Such an electron in site i and spin σ is created by $d_{i\sigma}^\dagger = e_i^\dagger s_{i,-\sigma}$, if it is in the “upper-Hubbard-band”, and by $d_{i\sigma}^\dagger = \sigma s_{i\sigma}^\dagger h_i$, if it is in a Zhang-Rice-type “lower-Hubbard-band”. Here e_i and h_i are (“excession” and “holon”) fermion operators, and $s_{i\sigma}$ are (“spinon”) boson operators. These auxiliary operators have to satisfy the constraint: $e_i^\dagger e_i + h_i^\dagger h_i + \sum_\sigma s_{i\sigma}^\dagger s_{i\sigma} = 1$.

An auxiliary space is determined within which a chemical-potential-like Lagrange multiplier is introduced to impose the constraint on the average. Physical observables are projected into the physical space by expressing them as combinations of Green’s functions of the auxiliary space. Since the time evolution of Green’s functions is determined by the Hamiltonian under which the constraint is obeyed rigorously, it is not expected to be violated as long as justifiable approximations are used.

Some of the material presented here, as well as further material about transport properties, has been published earlier [5].

II. UNCOUPLED AUXILIARY FIELDS

The uncoupled spinon field is diagonalized by applying the Bogoliubov transformation for bosons [6]: $s_\sigma(\mathbf{k}) = \cosh(\xi_{\sigma\mathbf{k}})\zeta_\sigma(\mathbf{k}) + \sinh(\xi_{\sigma\mathbf{k}})\zeta_{-\sigma}^\dagger(-\mathbf{k})$. The operators $\zeta_\sigma^\dagger(\mathbf{k})$ create spinon states of “bare” energies $\epsilon^\zeta(\mathbf{k})$ which have a V-shape zero minimum at $\mathbf{k} = \mathbf{k}_0$. Bose condensation results in AF order at wave vector $\mathbf{Q} = 2\mathbf{k}_0 = \mathbf{Q} = (\frac{\pi}{a}, \frac{\pi}{a})$. The values of \mathbf{k} are within the lattice Brillouin zone (BZ) [7], within which there are four inequivalent possibilities for \mathbf{k}_0 : $\pm(\frac{\pi}{2a}, \frac{\pi}{2a})$ and $\pm(\frac{\pi}{2a}, -\frac{\pi}{2a})$, thus introducing a broken symmetry. One has $\cosh(\xi_{\mathbf{k}}) \cong -\sinh(\xi_{\mathbf{k}}) \gg 1$ for $\mathbf{k} \rightarrow \mathbf{k}_0$ [6].

The adiabatic approximation is used concerning the dynamics of the stripe-like inhomogeneities, which are treated as static with respect to the

electrons dynamics. Within the one dimensional charged stripes it is justified to use the spin-charge separation approximation under which two-particle spinon-holon (spinon-excession) Green's functions are decoupled into single-auxiliary-particle Green's functions, resulting in the existence of a physical interpretation for the auxiliary particles. Holons (excessions) within the charged stripes are referred to as "stripions". Their creation operators (creating charge $-e$) are denoted by $p_{\mu}^{\dagger}(\mathbf{k})$, and bare energies by $\epsilon_{\mu}^p(\mathbf{k})$.

Because of the disordered one-dimensional nature of the charged stripes, it is found appropriate to assume localized uncoupled stripion states. Their \mathbf{k} wave vectors present \mathbf{k} -symmetrized combinations of degenerate localized states to be treated in a perturbation expansion. They are determined within a BZ based on periodic supercells which are large enough to approximately contain (each) the entire spectrum ϵ_{μ}^p of bare stripion energies.

Away from the charged stripes, creation operators of approximate fermion basis states of coupled holon-spinon and excision-spinon pairs are constructed, within the auxiliary space, as follows:

$$f_{\lambda\sigma}^{\dagger}(\mathbf{k}', \mathbf{k}) = \frac{e_{\lambda}^{\dagger}(\mathbf{k}')s_{\lambda,-\sigma}(\mathbf{k}' - \mathbf{k})}{\sqrt{n_{\lambda}^e(\mathbf{k}') + n_{\lambda,-\sigma}^s(\mathbf{k}' - \mathbf{k})}}, \quad (1)$$

$$g_{\lambda\sigma}^{\dagger}(\mathbf{k}', \mathbf{k}) = \frac{\sigma h_{\lambda}(\mathbf{k}')s_{\lambda\sigma}^{\dagger}(\mathbf{k} - \mathbf{k}')}{\sqrt{n_{\lambda}^h(\mathbf{k}') + n_{\lambda\sigma}^s(\mathbf{k} - \mathbf{k}')}}, \quad (2)$$

where \mathbf{k} and \mathbf{k}' are within the lattice BZ, the index λ accounts for the structure of the unit cell, and: $n_{\lambda}^e(\mathbf{k}) \equiv \langle e_{\lambda}^{\dagger}(\mathbf{k})e_{\lambda}(\mathbf{k}) \rangle$, $n_{\lambda}^h(\mathbf{k}) \equiv \langle h_{\lambda}^{\dagger}(\mathbf{k})h_{\lambda}(\mathbf{k}) \rangle$, $n_{\lambda\sigma}^s(\mathbf{k}) \equiv \langle s_{\lambda\sigma}^{\dagger}(\mathbf{k})s_{\lambda\sigma}(\mathbf{k}) \rangle$.

The states created by $f_{\lambda\sigma}^{\dagger}(\mathbf{k}', \mathbf{k})$ and $g_{\lambda\sigma}^{\dagger}(\mathbf{k}', \mathbf{k})$ have to be orthogonalized to the stripion states, and depleted to avoid over-completeness. Together with the small- U states [created by $c_{\nu\sigma}^{\dagger}(\mathbf{k})$] they form, within the auxiliary space, a basis to "quasi-electron" (QE) states whose creation operators are expressed as combinations:

$$q_{\nu\sigma}^{\dagger}(\mathbf{k}) = \sum_{\nu} U_{\nu\nu}^{cq}(\sigma\mathbf{k})^* c_{\nu\sigma}^{\dagger}(\mathbf{k}) + \sum_{\lambda\mathbf{k}'} [U_{\lambda\nu}^{fq}(\sigma\mathbf{k}', \sigma\mathbf{k})^* \times f_{\lambda\sigma}^{\dagger}(\mathbf{k}', \mathbf{k}) + U_{\lambda\nu}^{gq}(\sigma\mathbf{k}', \sigma\mathbf{k})^* g_{\lambda\sigma}^{\dagger}(\mathbf{k}', \mathbf{k})], \quad (3)$$

where the U coefficients are the eigenvector elements obtained in the diagonalization of the Hamiltonian within a mean-field approximation (and no coupling to the stripion and spinon fields). The obtained eigenvalues are the bare QE energies $\epsilon_{\nu}^q(\mathbf{k})$ which form quasi-continuous ranges of bands within the BZ around E_F [8].

III. COUPLED AUXILIARY FIELDS

Hopping and hybridization terms introduce strong coupling between the QE, stripion and spinon fields. It can be expressed in terms of a coupling Hamiltonian whose parameters can be in principle derived self-consistently from the original Hamiltonian. For p-type cuprates this coupling Hamiltonian can be expressed as:

$$\mathcal{H}' = \frac{1}{\sqrt{N}} \sum_{\iota\lambda\mu\sigma} \sum_{\mathbf{k}, \mathbf{k}'} \{ \sigma \epsilon_{\iota\lambda\mu}^{qp}(\sigma\mathbf{k}, \sigma\mathbf{k}') q_{\iota\sigma}^{\dagger}(\mathbf{k}) p_{\mu}(\mathbf{k}') \times [\cosh(\xi_{\lambda,\sigma(\mathbf{k}-\mathbf{k}')}) \zeta_{\lambda\sigma}(\mathbf{k} - \mathbf{k}') + \sinh(\xi_{\lambda,\sigma(\mathbf{k}-\mathbf{k}')}) \zeta_{\lambda,-\sigma}^{\dagger}(\mathbf{k}' - \mathbf{k})] + h.c. \}. \quad (4)$$

Here \mathbf{k} is within the stripions BZ, where the lattice BZ has been embedded, redefining the band indices of the QE's and the spinons appropriately. Using the Green's functions formalism, the QE, stripion and spinon propagators are coupled by a vertex introduced through \mathcal{H}' [9].

The stripe-like inhomogeneities involve the lattice [10] due to its coupling to the stripions. Consequently, processes (induced by \mathcal{H}') involving a transitions between stripion and QE states, followed by the emission and/or absorption of spinons, should involve also the emission and/or absorption of phonons. This can be expressed by multiplying a spinon propagator, in such processes, by a power series of phonon propagators [9]. Such a phonon-"dressed" spinon is referred to as a "svivon", carrying spin and lattice distortion, and it replaces the spinon in the \mathcal{H}' vertex.

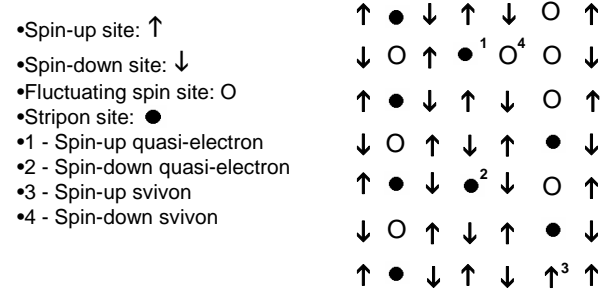


FIG. 1. An adiabatic "snapshot" of a stripe-like inhomogeneity and carriers within a CuO_2 plane.

An adiabatic "snapshot" of a CuO_2 plane with a stripe-like inhomogeneity, and physical realizations of the auxiliary fields in the plane, within the $t-t'-J$ model, is shown in Fig. 1. Within the adiabatic time scale a site is "spinless" either if the spin on it is replaced by charge, removing the electron or the hole carrying that spin (as in "stripion sites" in Fig. 1), or if the spin is fluctuating on a shorter

time scale (due to, *e.g.*, being in fluctuating singlet spin pairs). A site stripon excitation represents a transition between these two types of a spinless site within the charged stripes. A site svivon excitation represents a transition between a spinned site and a fluctuating-spin spinless site. A site QE excitation represents a transition between a spinned site and a charged spinless site within the AF stripes. For simplicity we ignore in Fig. 1 the dynamics of the QE, stripon, and svivon sites (whose time scale is shorter than the adiabatic time scale).

The Green's functions \mathcal{G} of the auxiliary fields are approached through the spectral functions $A_l^q(\mathbf{k}, \omega)$, $A_\mu^p(\mathbf{k}, \omega)$, and $A_\lambda^\zeta(\mathbf{k}, \omega)$ for the QE's, stripions, and svivons, respectively [$A(\omega) \equiv \Im \mathcal{G}(\omega - i0^+)/\pi$]. The solution studied (see below) has a considerably smaller stripon bandwidth than the QE and svivon bandwidths; thus a phase-space argument can be used, as in the Migdal theorem, to prove that vertex corrections to the \mathcal{H}' vertex are negligible. The resulting diagrams [9] for the self-energy Σ yield the following expressions for the QE, stripon, and svivon scattering rates $\Gamma^q(\mathbf{k}, \omega)$, $\Gamma^p(\mathbf{k}, \omega)$, and $\Gamma^\zeta(\mathbf{k}, \omega)$ [$\Gamma(\mathbf{k}, \omega) \equiv 2\Im\Sigma(\mathbf{k}, \omega - i0^+)$]:

$$\begin{aligned} \Gamma_{\nu\nu'}^q(\mathbf{k}, \omega) &\cong \frac{2\pi}{N} \sum_{\lambda\mu\mathbf{k}'} \int d\omega' \epsilon_{\nu\lambda\mu}^{qp}(\mathbf{k}', \mathbf{k}) \epsilon_{\nu'\lambda\mu}^{qp}(\mathbf{k}', \mathbf{k})^* \\ &\times A_\mu^p(\mathbf{k}', \omega') [-\cosh^2(\xi_{\lambda, \mathbf{k}-\mathbf{k}'}) A_\lambda^\zeta(\mathbf{k}-\mathbf{k}', \omega-\omega') \\ &+ \sinh^2(\xi_{\lambda, \mathbf{k}-\mathbf{k}'}) A_\lambda^\zeta(\mathbf{k}-\mathbf{k}', \omega'-\omega)] \\ &\times [f_T(\omega') + b_T(\omega'-\omega)], \end{aligned} \quad (5)$$

$$\begin{aligned} \Gamma_{\mu\mu'}^p(\mathbf{k}, \omega) &\cong \frac{2\pi}{N} \sum_{i\mathbf{k}'\sigma} \int d\omega' \epsilon_{i\lambda\mu}^{qp}(\mathbf{k}', \mathbf{k})^* \epsilon_{i\lambda\mu'}^{qp}(\mathbf{k}', \mathbf{k}) \\ &\times A_l^q(\mathbf{k}', \omega') [\cosh^2(\xi_{\lambda, \mathbf{k}'-\mathbf{k}}) A_\lambda^\zeta(\mathbf{k}'-\mathbf{k}, \omega'-\omega) \\ &- \sinh^2(\xi_{\lambda, \mathbf{k}'-\mathbf{k}}) A_\lambda^\zeta(\mathbf{k}'-\mathbf{k}, \omega-\omega')] \\ &\times [f_T(\omega') + b_T(\omega'-\omega)], \end{aligned} \quad (6)$$

$$\begin{aligned} \Gamma_{\lambda\lambda'}^\zeta(\mathbf{k}, \omega) &\cong \frac{2\pi}{N} \sum_{i\mathbf{k}'\mu} \int d\omega' \epsilon_{i\lambda\mu}^{qp}(\mathbf{k}', \mathbf{k}'-\mathbf{k})^* \\ &\times \epsilon_{i\lambda'\mu}^{qp}(\mathbf{k}', \mathbf{k}'-\mathbf{k}) [\cosh(\xi_{\lambda\mathbf{k}}) \cosh(\xi_{\lambda'\mathbf{k}}) A_l^q(\mathbf{k}', \omega') \\ &\times A_\mu^p(\mathbf{k}'-\mathbf{k}, \omega'-\omega) + \sinh(\xi_{\lambda\mathbf{k}}) \sinh(\xi_{\lambda'\mathbf{k}}) \\ &\times A_l^q(\mathbf{k}', -\omega') A_\mu^p(\mathbf{k}'-\mathbf{k}, \omega-\omega')] \\ &\times [f_T(\omega'-\omega) - f_T(\omega')], \end{aligned} \quad (7)$$

where $f_T(\omega)$ and $b_T(\omega)$ are the Fermi and Bose distribution functions at temperature T .

The real parts of the self energies and the spectral functions (based on the diagonal self-energy terms) are obtained from the above expressions through:

$$\Re\Sigma(\mathbf{k}, \omega) = \wp \int \frac{d\omega' \Gamma(\mathbf{k}, \omega')}{2\pi(\omega - \omega')}, \quad (8)$$

$$A(\mathbf{k}, \omega) = \frac{\Gamma(\mathbf{k}, \omega)/2\pi}{[\omega - \epsilon(\mathbf{k}) - \Re\Sigma(\mathbf{k}, \omega)]^2 + [\Gamma(\mathbf{k}, \omega)/2]^2}. \quad (9)$$

IV. AUXILIARY SPECTRAL FUNCTIONS

A self-consistent solution is obtained, and expressions are derived below for the intermediary energy range. The high energy range ($\gtrsim 0.5$ eV), determined by the hopping and exchange parameters, is treated by introducing cut-off integration limits at $\pm\omega_c$ to the integrals (resulting in spurious logarithmic divergencies at $\pm\omega_c$). The solution includes a low energy range ($\lesssim 0.02$ eV), appearing in these expressions as “zero-energy” non-analytic behavior. Ignoring the variation of the matrix elements in Eqs. (5–7), and omitting the dependence on \mathbf{k} for simplicity, the sums of the auxiliary spectral functions over the band indices and small \mathbf{k}' ranges can be expressed, self-consistently, as (all the coefficients are positive):

$$\tilde{A}^q(\omega) \cong \begin{cases} a_+^q \omega + b_+^q, & \text{for } \omega > 0, \\ -a_-^q \omega + b_-^q, & \text{for } \omega < 0, \end{cases} \quad (10)$$

$$\tilde{A}^p(\omega) \cong \delta(\omega), \quad (11)$$

$$\tilde{A}^\zeta(\omega) \cong \begin{cases} a_+^\zeta \omega + b_+^\zeta, & \text{for } \omega > 0, \\ a_-^\zeta \omega - b_-^\zeta, & \text{for } \omega < 0. \end{cases} \quad (12)$$

Analyticity is expected to be restored in the low-energy range, and specifically $\tilde{A}^\zeta(\omega = 0) = 0$. Also special behavior is expected for svivons around \mathbf{k}_0 . By inserting these terms in Eqs. (5–7), the following expressions are derived, assuming the low T limits for $f_T(\omega)$ and $b_T(\omega)$ (again all the coefficients are positive):

$$\frac{\Gamma^q(\omega)}{2\pi} \cong \begin{cases} c_+^q \omega + d_+^q, & \text{for } \omega > 0, \\ -c_-^q \omega + d_-^q, & \text{for } \omega < 0, \end{cases} \quad (13)$$

$$\frac{\Gamma^p(\omega)}{2\pi} \cong \begin{cases} c_+^p \omega^3 + d_+^p \omega^2 + e_+^p \omega, & \text{for } \omega > 0, \\ -c_-^p \omega^3 + d_-^p \omega^2 - e_-^p \omega, & \text{for } \omega < 0, \end{cases} \quad (14)$$

$$\frac{\Gamma^\zeta(\omega)}{2\pi} \cong \begin{cases} c_+^\zeta \omega + d_+^\zeta, & \text{for } \omega > 0, \\ c_-^\zeta \omega - d_-^\zeta, & \text{for } \omega < 0. \end{cases} \quad (15)$$

Integrating through Eq. (8) (between the limits $\pm\omega_c$) results in:

$$\begin{aligned} -\Re\Sigma^q(\omega) &\cong \omega_c(c_+^q - c_-^q) + (d_+^q \ln \left| \frac{\omega - \omega_c}{\omega} \right| \\ &- d_-^q \ln \left| \frac{\omega + \omega_c}{\omega} \right|) + \omega(c_+^q \ln \left| \frac{\omega - \omega_c}{\omega} \right| \\ &+ c_-^q \ln \left| \frac{\omega + \omega_c}{\omega} \right|), \end{aligned} \quad (16)$$

$$-\Re\Sigma^p(\omega) \cong \left[\frac{\omega_c^3}{3}(c_+^p - c_-^p) + \frac{\omega_c^2}{2}(d_+^p - d_-^p) \right]$$

$$\begin{aligned}
 & + \omega_c(e_+^p - e_-^p)] + \omega \left[\frac{\omega_c^2}{2} (c_+^p + c_-^p) \right. \\
 & + \omega_c(d_+^p + d_-^p) + e_+^p \ln \left| \frac{\omega - \omega_c}{\omega} \right| \\
 & + e_-^p \ln \left| \frac{\omega + \omega_c}{\omega} \right| \left. + \omega^2 [\omega_c(c_+^p - c_-^p) \right. \\
 & + d_+^p \ln \left| \frac{\omega - \omega_c}{\omega} \right| - d_-^p \ln \left| \frac{\omega + \omega_c}{\omega} \right| \left. \right] \\
 & + \omega^3 [c_+^p \ln \left| \frac{\omega - \omega_c}{\omega} \right| + c_-^p \ln \left| \frac{\omega + \omega_c}{\omega} \right|], \quad (17)
 \end{aligned}$$

$$\begin{aligned}
 -\Re\Sigma^\zeta(\omega) \cong & \omega_c(c_+^\zeta + c_-^\zeta) + (d_+^\zeta \ln \left| \frac{\omega - \omega_c}{\omega} \right| \\
 & + d_-^\zeta \ln \left| \frac{\omega + \omega_c}{\omega} \right|) + \omega (c_+^\zeta \ln \left| \frac{\omega - \omega_c}{\omega} \right| \\
 & - c_-^\zeta \ln \left| \frac{\omega + \omega_c}{\omega} \right|). \quad (18)
 \end{aligned}$$

Note that the logarithmic divergencies at $\omega = 0$ are truncated by analyticity in the low-energy range.

The resulting $\Re\Sigma$ renormalize the auxiliary-particle energies ϵ to: $\bar{\epsilon} = \epsilon + \Re\Sigma(\bar{\epsilon})$. The extent of the renormalization can be estimated through $d\bar{\epsilon}/d\epsilon = [1 - d\Re\Sigma(\bar{\epsilon})/d\bar{\epsilon}]^{-1}$. This renormalization is particularly strong for the stripon energies, due to the effect of the quasi-continuum of QE bands, reflected in a significant ω^3 term in $\Gamma^p(\omega)$ (14). It introduces a large negative term $-(c_+^p + c_-^p)\omega_c^2/2$ (17) to $d\Re\Sigma^p(\bar{\epsilon})/d\bar{\epsilon}$, resulting in a very small $d\bar{\epsilon}^p/d\epsilon^p$. Thus the stripon bandwidth drops down to the low energy range, and a δ -function is appropriate for $\tilde{A}^p(\omega)$ (11).

Expressions (10), for $\tilde{A}^q(\omega)$, and (12) for $\tilde{A}^\zeta(\omega)$ result, through Eq. (9), from the effects of bands crossing zero energy, which mainly contribute to the constant (b) terms [due to the normalization of the spectral functions (9)], and of higher energy bands, whose effect through (9) is approximately $\propto \Gamma(\omega)$, and thus contribute to the constant (b) and linear (a) terms.

The self-consistent treatment introduces inequalities between positive and negative ω coefficients in Eqs. (10–15), resulting from the fact that the svivon spectrum has more weight for $\omega > 0$, and that [in Eqs. (5–7)] $\cosh^2(\xi_{\mathbf{k}}) > \sinh^2(\xi_{\mathbf{k}})$. For the case of p-type cuprates (worked out in these equation) the following inequalities are built up self-consistently:

$$a_+^q > a_-^q, \quad b_+^q > b_-^q, \quad c_+^q > c_-^q, \quad d_+^q > d_-^q, \quad (19)$$

$$a_+^\zeta > a_-^\zeta, \quad b_+^\zeta > b_-^\zeta, \quad c_+^\zeta > c_-^\zeta, \quad d_+^\zeta > d_-^\zeta. \quad (20)$$

For “real” n-type cuprates, in which the stripions are based on excitation and not holon states, the roles of $\cosh(\xi_{\mathbf{k}})$ and $\sinh(\xi_{\mathbf{k}})$ are reversed in \mathcal{H}' (4), and in the expressions derived from it. consequently the direction of the inequalities is reversed for the QE coefficients (19), but stays the same for

the svivon coefficients (20). One could expect deviations from the inequalities (19–20) at specific \mathbf{k} points; they almost disappear for svivons close to point \mathbf{k}_0 , where $\cosh(\xi_{\mathbf{k}}) \cong -\sinh(\xi_{\mathbf{k}})$ [6], and for QE’s coupled mainly to such svivons.

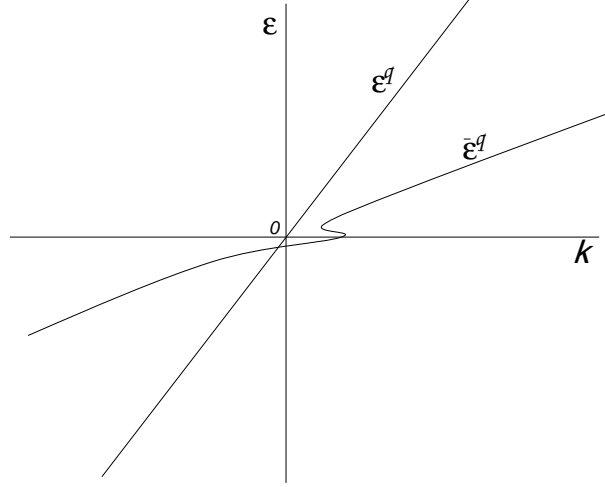


FIG. 2. A typical self-energy renormalization of the QE energies, for p-type cuprates.

A typical renormalization of the QE energies (for p-type cuprates), around zero energy, is shown in Fig. 2. One renormalization effect is a reduction of the band slope. Another effect is a consequence of the logarithmic singularity (truncated in the low-energy range) in $\Re\Sigma^q$ at $\omega = 0$, due to the $(d_+^q - d_-^q) \ln |\omega|$ term in Eq. (16). The asymmetry between positive and negative energies is a consequence of inequality (19), and this asymmetry is expected to be inverted for “real” n-type cuprates.

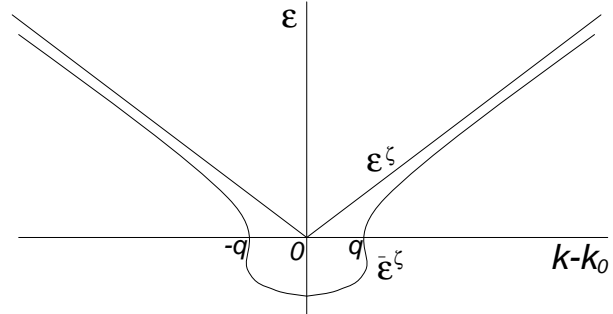


FIG. 3. A typical self-energy renormalization of the svivon energies around the minimum at \mathbf{k}_0 .

A typical renormalization of the svivon energies, around the V-shape zero minimum of ϵ^ζ at \mathbf{k}_0 , is shown in Fig. 3. A major renormalization effect is due to the $(d_+^\zeta + d_-^\zeta) \ln |\omega|$ term in $\Re\Sigma^\zeta(\omega)$ (18), contributing a logarithmic singularity (truncated in the low-energy range) at $\omega = 0$. By Eq. (15) $\bar{\epsilon}^\zeta$ is ex-

pected to have a considerable linewidth around \mathbf{k}_0 (except where it crosses zero). This changes when a pairing gap in low-energy QE and stripon states (coupled by svivons around \mathbf{k}_0) disables the scattering processes causing linewidth (7) near the negative minimum of $\bar{\epsilon}^\zeta$ at \mathbf{k}_0 .

This renormalization of the svivon energies changes the physical signature of their Bose condensation from AF order to the observed stripe-like inhomogeneities. The exact low-energy details around the minimum in $\bar{\epsilon}^\zeta$ determine, self-consistently, the nature of these inhomogeneities. The dynamics of these inhomogeneities depends on the linewidth of $\bar{\epsilon}^\zeta(\mathbf{k}_0)$ around \mathbf{k}_0 , and thus becomes slower in pairing states (where they can be observed). The crossover energy from the intermediary to the low energy range is determined by $|\bar{\epsilon}^\zeta(\mathbf{k}_0)|$ and the stripon bandwidth ω^p .

V. ELECTRON SPECTRUM

Spectroscopies, like ARPES, measuring the effect of transfer of electrons into, or out of, the crystal, are determined by $A_e(\mathbf{p}, \omega) \equiv \Im \mathcal{G}_e(\mathbf{p}, \omega - i0^+)/\pi$, the electrons spectral function at momentum \mathbf{p} and energy ω . They are expressed in terms of the auxiliary space spectral functions in Eqs. (10–12), thus being projected from the auxiliary to the physical space. Denoting by $\langle \mathbf{p} | \phi(\mathbf{k}) \rangle$ the \mathbf{p} -Fourier transforms of specified electron wave functions, A_e can be expressed as:

$$\begin{aligned}
 A_e(\mathbf{p}, \omega) = & \sum_{\mathbf{k}\sigma} \left\{ \sum_{\iota} A_{\iota}^q(\mathbf{k}, \omega) \left[\sum_{\nu} |\langle \mathbf{p} | \phi_{\nu}^e(\mathbf{k}) \rangle|^2 \right. \right. \\
 & \times |U_{\nu\iota}^{cq}(\mathbf{k})|^2 + \frac{1}{N} \sum_{\lambda\mathbf{k}'\mathbf{k}''} [|\langle \mathbf{p} | \phi_{\lambda}^f(\mathbf{k}) \rangle|^2 U_{\lambda\iota}^{fq}(\mathbf{k}', \mathbf{k})^* \\
 & \times U_{\lambda\iota}^{fq}(\mathbf{k}'', \mathbf{k}) \sqrt{n_{\lambda}^e(\mathbf{k}') + n_{\lambda, -\sigma}^s(\mathbf{k}' - \mathbf{k})} \\
 & \times \sqrt{n_{\lambda}^e(\mathbf{k}'') + n_{\lambda, -\sigma}^s(\mathbf{k}'' - \mathbf{k}) + |\langle \mathbf{p} | \phi_{\lambda}^g(\mathbf{k}) \rangle|^2} \\
 & \times U_{\lambda\iota}^{gq}(\mathbf{k}', \mathbf{k})^* U_{\lambda\iota}^{gq}(\mathbf{k}'', \mathbf{k}) \sqrt{n_{\lambda}^h(\mathbf{k}') + n_{\lambda\sigma}^s(\mathbf{k} - \mathbf{k}')} \\
 & \times \left. \left. \sqrt{n_{\lambda}^h(\mathbf{k}'') + n_{\lambda\sigma}^s(\mathbf{k} - \mathbf{k}'')} \right] \right\} \\
 & + \frac{1}{N} \sum_{\lambda\mu\mathbf{k}'} |\langle \mathbf{p} | \phi_{\lambda\mu}^{\zeta p}(\mathbf{k}) \rangle|^2 \int d\omega' A_{\mu}^p(\mathbf{k}', \omega') \\
 & \times [-\cosh^2(\xi_{\lambda, \mathbf{k}-\mathbf{k}'} A_{\lambda}^{\zeta}(\mathbf{k} - \mathbf{k}', \omega - \omega')) \\
 & + \sinh^2(\xi_{\lambda, \mathbf{k}-\mathbf{k}'} A_{\lambda}^{\zeta}(\mathbf{k} - \mathbf{k}', \omega' - \omega))] \\
 & \times [f_T(\omega') + b_T(\omega' - \omega)]. \quad (21)
 \end{aligned}$$

Note that A_e is expressed here in terms of A_{ι}^q and $A_{\lambda}^{\zeta} A_{\mu}^p$, corresponding to diagonal elements of the

auxiliary space Green's functions in the basis of the eigenstates of the bare auxiliary fields. The electron bands are based on eigenstates of the coupled-fields system, where \mathcal{H}' (4) introduces hybridization between QE (ι) and svivon-stripon ($\lambda\mu$) states.

The $n_{\lambda}^e + n_{\lambda\sigma}^s$ ($n_{\lambda}^h + n_{\lambda\sigma}^s$) terms in Eq. (21) represent a large- U effect discussed in Ref. [11]. When all the sites are unoccupied by large- U electrons (holes), then $n_{\lambda\sigma}^s = 0$, $n_{\lambda}^e = 1$ ($n_{\lambda}^h = 1$), and the above terms contribute a factor one in A_e , reflecting the fact that there is spectral weight for both spin states per site in the lower (upper) Hubbard band. On the other hand, when each site is occupied by a large- U electron (hole), then $n_{\lambda\sigma}^s = \frac{1}{2}$ (for both spins), $n_{\lambda}^e = n_{\lambda}^h = 0$, and the above terms contribute factors half in A_e , reflecting the fact that there is spectral weight for one electron (hole) state per site, in both the lower and the upper Hubbard bands.

An important question is how the quasi-continuum of QE bands is projected into physical electron bands. The eigenvector elements $U_{\lambda\iota}^{fq}$ and $U_{\lambda\iota}^{gq}$ appearing in Eq. (21) are of order $1/\sqrt{N}$, and their phases are quite random. Consequently almost all the QE (ι) bands have a contribution of order $1/N$ to an ‘‘incoherent’’ background of A_e . A contribution of ‘‘coherent’’ bands to A_e , in the vicinity of E_F comes from few QE bands for which $U_{\nu\iota}^{cq} \sim 1$, or for which almost all $U_{\lambda\iota}^{fq}$ or $U_{\lambda\iota}^{gq}$ have the same phase. These bands correspond to QE's which are closely related to physical electrons.

Eq. (21) preserves the auxiliary-space ω dependencies (10–20) for the physical spectral functions (both in the coherent bands, and in the incoherent background). The results for Γ^q in Eq. (13) are reflected in non-Fermi-liquid linewidths, having a $\propto \omega$ and a constant term, as detected in ARPES results [12]. The convoluted stripon–svivon term in Eq. (21) hybridizes both with the incoherent background, and the coherent bands. Since this term (in A_e) is similar to the expression for Γ^q in Eq. (5), its ω dependence has [similarly to Eq. (13)] a $\propto \omega$ and a constant term, as that of the QE contribution to A_e [given by Eq. (13)].

The fact that the stripions introduce lower periodicity to the QE's and svivons, they are coupled to, is experimentally reflected in ‘‘shadow bands’’ and other weak-intensity superstructure effects. The strongest coupling is expected for svivons around \mathbf{k}_0 (see the behavior of $\bar{\epsilon}^\zeta$ there in Fig. 3), and for QE's at BZ areas of dominantly high electrons density of states (DOS), found in the LSCO, BSCCO and TBCO systems around the ‘‘antinodal’’ points $(\frac{\pi}{a}, 0)$ and $(0, \frac{\pi}{a})$. If (from its four possibilities) \mathbf{k}_0 were chosen at $(\frac{\pi}{2a}, \frac{\pi}{2a})$, then the areas in the lattice

BZ which the stripon states reside in (at least in the above systems) would be around $\pm \mathbf{k}^p = \pm(\frac{\pi}{2a}, -\frac{\pi}{2a})$ [13] (the antinodal points are at $\mathbf{k}^p \pm \mathbf{k}_0$). Thus one finds in BZ ranges around the antinodal points a stripon–svivon contribution to A_e which is very close to E_F (at energies $\bar{\epsilon}^p \pm \bar{\epsilon}^\zeta$ of considerable linewidths). Such behavior in antinodal areas has been widely observed (see *e.g.* Ref. [14]). The opening of an SC gap decreases the linewidth of $\bar{\epsilon}^\zeta$ near \mathbf{k}_0 (see Fig. 3) resulting in narrow antinodal $\bar{\epsilon}^p \pm \bar{\epsilon}^\zeta$ states, as will be discussed below.

The renormalization of the QE energies, shown in Fig. 2, is expected to occur for electron bands projected from them. Thus the experimentally observed band slopes are smaller than the LDA predictions. Also, the effect of the logarithmic singularity in Fig. 2 has been observed in ARPES as a “kink” [15,16] in the “nodal” band as E_F is approached from below [near point $(\frac{\pi}{2a}, \frac{\pi}{2a})$ in the BZ]. But it was attributed to coupling to phonons [15] or to the neutron scattering resonance mode [16]. Note, however, that such a coupling would generally result in two opposite changes in the band slope (below and above the coupled excitation energy) below E_F , while the experimental kink looks more consistent with one change in slope below E_F , as in Fig. 2. Also, QE’s close to the nodal points are expected to be coupled to svivons which are mostly fairly away from point \mathbf{k}_0 , and thus the inequalities (19–20), which are necessary for this logarithmic singularity to occur, are significant.

This kink was not found in measurements in the n-type cuprate NCCO [17], which is consistent with the prediction here (suggested by the author earlier [5]) that in “real” n-type cuprates this kink should be above, and not below E_F (where ARPES measurements are relevant). Also, there appears to be a sharp upturn in the ARPES band in NCCO [17] very close to E_F (believed there to be an artifact), which is expected here as the kink is approached from the other side of E_F (see Fig. 2).

VI. THE NEUTRON RESONANCE MODE

Spectroscopies measuring spin-flip excitations are largely determined by terms like $\langle s_{i\sigma}^\dagger s_{i,-\sigma} s_{j,-\sigma} s_{j\sigma}^\dagger \rangle$, contributing the following term to the imaginary part of the spin susceptibility at wave vector \mathbf{q} (within the lattice BZ) and energy ω :

$$\chi''(\mathbf{q}, \omega) \sim \sum_{\mathbf{k}} \sinh(2\xi_{\mathbf{k}}) \sinh(2\xi_{\mathbf{q}-\mathbf{k}}) \\ \times \int d\omega' A^\zeta(\mathbf{k}, \omega') \{A^\zeta(\mathbf{q}-\mathbf{k}, -\omega-\omega')$$

$$- A^\zeta(\mathbf{q}-\mathbf{k}, \omega-\omega') + 2A^\zeta(\mathbf{q}-\mathbf{k}, \omega'-\omega) \\ \times [b_T(\omega'-\omega) - b_T(\omega')]\}. \quad (22)$$

The effect of the negative minimum of $\bar{\epsilon}^\zeta(\mathbf{k})$ at \mathbf{k}_0 , in Fig. 3, and especially in the SC state, where its linewidth is small, is the existence of a peak in $\chi''(\mathbf{q}, \omega)$ at $\mathbf{q} = 2\mathbf{k}_0 = \mathbf{Q}$ (the AF wave vector) and $\omega = -2\bar{\epsilon}^\zeta(\mathbf{k}_0)$.

This peak is consistent with the neutron-scattering resonance [thus $E_{\text{res}} = -2\bar{\epsilon}^\zeta(\mathbf{k}_0)$] found in the high- T_c cuprate at ~ 0.04 eV [18–21]. The observation that the energy of the neutron resonance mode has a local maximum at $\mathbf{k} = \mathbf{Q}$ is also consistent with Fig. 3 and Eq. (22). However, also a peak whose energy is rising with $\mathbf{k} - \mathbf{Q}$ is expected due to the range where $\bar{\epsilon}^\zeta(\mathbf{k})$ is positive and rising. And indeed, recent measurements [22] show neutron-scattering peak branches dispersing both downward and upward with approximate circular symmetry around $\mathbf{k} = \mathbf{Q}$, as expected here. The incommensurate low-energy neutron-scattering peaks, corresponding to the stripe-like inhomogeneities [2], occur at points $\mathbf{Q} \pm 2\mathbf{q}$, in directions where $\bar{\epsilon}^\zeta(\mathbf{k}_0 \pm \mathbf{q}) = 0$, and the slope of $\bar{\epsilon}^\zeta(\mathbf{k})$ at $\mathbf{k}_0 \pm \mathbf{q}$ (see Fig. 3) is not too steep.

Except for the single-layer TBCO, the resonance mode has been observed in bilayer cuprates, where its symmetry is odd with respect to the layers exchange. For two exchange-coupled CuO_2 planes [7], the bare spinon energies split into “acoustic” (with a V-shape zero minimum) and “optical” bands, of odd and even symmetries, respectively. In an AF phase, double-spinon excitations of these modes result in acoustic and optical spin-wave modes, as has been observed [23]. The self energy renormalization, resulting in a negative minimal svivon energy, demonstrated in Fig. 3, is relevant to the (odd) acoustic mode [where $\bar{\epsilon}_o^\zeta(\mathbf{k}_0) < 0$], while the renormalization of the (even) optical mode is a minor shift, resulting in a minimal energy $\bar{\epsilon}_e^\zeta(\mathbf{k}_0) > 0$. Generalizing Eq. (22) to the bilayer case yields the neutron resonance peak for odd symmetry, around energy $E_{\text{res}} = -2\bar{\epsilon}_o^\zeta(\mathbf{k}_0)$ at $\mathbf{k} = \mathbf{Q}$, as discussed above, while for even symmetry one expects a higher energy peak, whose minimal energy $2\bar{\epsilon}_e^\zeta(\mathbf{k}_0)$ is at $\mathbf{k} = \mathbf{Q}$. This is consistent with high-energy neutron-scattering measurements [24].

Thus, the neutron resonance mode is an excitation towards the destruction of the stripe-like inhomogeneities, and its width determines the speed of their dynamics. $E_{\text{res}}/2$ is an indicator of the low-energy scale. Transport properties, and especially thermoelectric power, are sensitive to another indicator of the low-energy scale, the stripon bandwidth. Expressions for them were worked out in

Ref. [5], from which also this bandwidth was found to be $\omega^p \sim 0.02$ eV.

VII. STRIPON HOPPING PROCESSES

A major consequence of the coupling between the stripon, svivon, and QE fields (worked out above) is stripon hopping between different charged stripes, through intermediary QE+svivon states. Adiabatic snapshots of consecutive steps in such inter-stripe hopping scenarios, within the same section of stripe-like inhomogeneity as in Fig. 1, are shown in Figs. 4,5. Dynamics of carriers beside those demonstrating the hopping steps is ignored for simplicity.

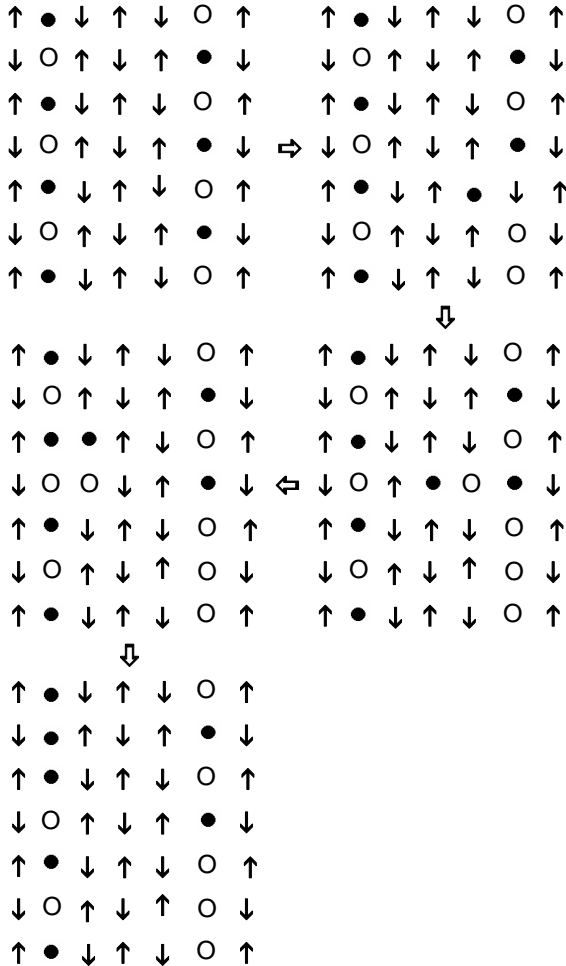


FIG. 4. Adiabatic snapshots of consecutive steps in a scenario for “ t' -induced” inter-stripe stripon hopping via QE+svivon states.

Within the t - t' - J model inter-site hopping could be either between nearest neighbors (t -induced), or between next nearest neighbors (t' -induced). The

inter-stripe stripon hopping scenarios illustrated in Fig. 4 and Fig. 5 are through four consecutive t' -induced and t -induced inter-site hopping steps, respectively. The intermediary states are of QE's and svivons, where the latter propagate through spin (and lattice) dynamics.

There is a difference between the dependencies of these two types of inter-stripe hopping processes on the stripe structure. The t' -induced hopping could occur in a similar manner to that illustrated in Fig. 4 also if the AF stripes were wider, and also in the case of “diagonal stripes”, existing in lightly doped (non-SC) cuprates. On the other hand, t -induced hopping, as illustrated in Fig. 5, is specific to the shown case of four-sites separation between the charged stripes, and would involve higher energy intermediary states for wider AF stripes, or diagonal stripes. Thus t -induced inter-stripe hopping should be less effective for low doping levels.

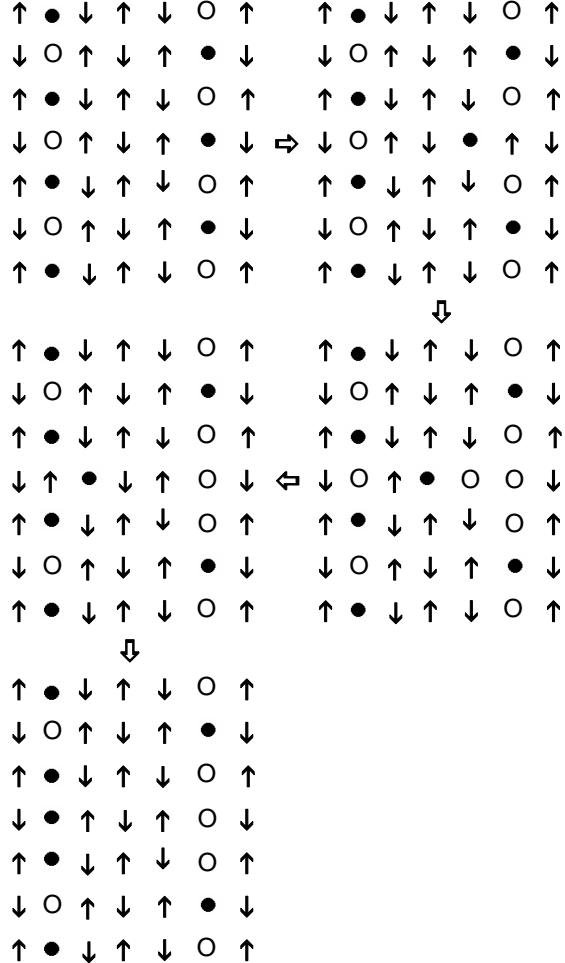


FIG. 5. Adiabatic snapshots of consecutive steps in a scenario for “ t -induced” inter-stripe stripon hopping via QE+svivon states.

This is consistent with the evolution of the metallic behavior of LSCO with doping observed in ARPES measurements [25]. For low doping levels x the stripes are diagonal, and inter-stripe hopping is mainly t' -induced, resulting in the observed [25] appearance of nodal states on E_F . For higher x the stripes become oriented as in Fig. 1, with the distance between charged stripes being small enough for t -induced inter-stripe hopping to contribute substantially. This results in the observed [25] appearance of antinodal states on E_F , and SC.

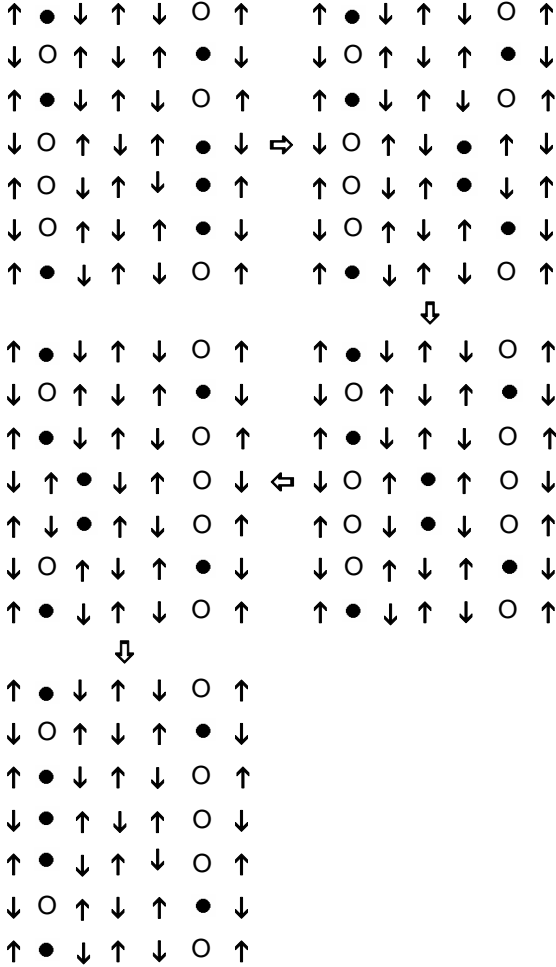


FIG. 6. Adiabatic snapshots of consecutive steps in a scenario for inter-stripe hopping of stripon pairs via QE pair states.

VIII. HOPPING-INDUCED PAIRING

It has been pointed out by the author [5,9] that the electronic structure discussed here provides pairing due to transitions between pair states of stripons and QE's through the exchange of svivons

(the pairing diagram is sketched in Ref. [9]). A scenario for inter-stripe pair hopping, contributing to such pairing, is illustrated in Fig. 6. The starting (ending) steps in this pair-hopping scenario is a t -hopping of a nearest-neighbor “dressed” stripon pair, followed (preceded) by turning this pair into (from) a pair of nearest-neighbor QE's, through the exchange of a svivon [consisting of turning a pair of nearest-neighbor opposite spins into (from) a singlet pair of fluctuating spins]. The two intermediary steps consist of hopping of the nearest-neighbor QE pair, which could be either t' -hopping or t -hopping with nearest-neighbor spin-flip [26]. Note that t' -hopping allows also scenarios where the QE pair gets apart and joins again with no svivon excitation. Also note that such pairing scenarios do not occur for diagonal stripes.

Such pair-hopping scenarios result in gain in inter-stripe hopping energy, compared to the single-particle inter-stripe hopping scenarios, sketched in Figs. 4,5, avoiding intermediary svivon excitations. Furthermore, hybridization with other orbitals, beyond the $t-t'-J$ model, results in further gain in (both intra-plane and inter-plane) hopping energy, since it enables the QE pair to move from the CuO_2 plane section shown in Fig. 6, to another section which may be in another CuO_2 plane.

The pairing diagram [9] leads to Eliasherg-type equations, of coupled stripon and QE pairing order parameters. Coherent pairing should be between two subsets of the QE's and stripons. For QE's these subsets are, naturally, chosen to be those of the spin-up (\uparrow) and spin-down (\downarrow) QE's. As was illustrated in Fig. 1, for a CuO_2 plane within the $t-t'-J$ model the \uparrow bare QE's can reside on \downarrow sites, and the \downarrow bare QE's can reside on \uparrow sites of the stripe-like inhomogeneities.

An adiabatic snapshot of an extended section of a stripe-like inhomogeneity, including an expected crossover between stripe segments directed in the a and the b directions, is shown in Fig. 7. Denoted are the available sites for the \uparrow and \downarrow QE subsets. The stripons are spinless, but since the QE subsets have a spatial interpretation in the CuO_2 planes, within the adiabatic time scale, it is logical to choose the stripon subsets also on a spatial basis, in a manner which optimizes pairing through scenarios similar to that illustrated in Fig. 6. Thus the pairing subsets are chosen for bare stripons such that the nearest neighbors (on a charged stripe) of a site corresponding to one subset are sites corresponding to the other subset. These subsets are denoted by Δ and ∇ , and the sites available for them are shown in Fig. 7 too.

The pairing order parameters are the QE and

stripon pair-correlation functions defined [in the position (\mathbf{r}) representation] as:

$$\Phi^q(\mathbf{r}_1, \mathbf{r}_2) \equiv \langle q_\uparrow(\mathbf{r}_1)q_\downarrow(\mathbf{r}_2) \rangle, \quad (23)$$

$$\Phi^p(\mathbf{r}_1, \mathbf{r}_2) \equiv \langle p_\Delta(\mathbf{r}_1)p_\nabla(\mathbf{r}_2) \rangle. \quad (24)$$

The coupled Eliashberg-type equations for these order parameters can be expressed (omitting band indices for simplicity), in the position and the Matsubara (ω_n) representations, as:

$$\begin{aligned} \Phi^q(\mathbf{r}_1, \mathbf{r}_2, i\omega_n) = & \sum_{n'} \int d\mathbf{r}'_1 \int d\mathbf{r}'_2 \\ & \times K^{qp}(\mathbf{r}_1, \mathbf{r}_2, n; \mathbf{r}'_1, \mathbf{r}'_2, n') \Phi^p(\mathbf{r}'_1, \mathbf{r}'_2, i\omega'_n), \end{aligned} \quad (25)$$

$$\begin{aligned} \Phi^p(\mathbf{r}_1, \mathbf{r}_2, i\omega_n) = & \sum_{n'} \int d\mathbf{r}'_1 \int d\mathbf{r}'_2 \\ & \times K^{pq}(\mathbf{r}_1, \mathbf{r}_2, n; \mathbf{r}'_1, \mathbf{r}'_2, n') \Phi^q(\mathbf{r}'_1, \mathbf{r}'_2, i\omega'_n). \end{aligned} \quad (26)$$

Expressions for the kernel functions K^{qp} and K^{pq} are obtained from the pairing diagrams. They depend on Φ^q and Φ^p up to the temperature where the latter vanish [27].

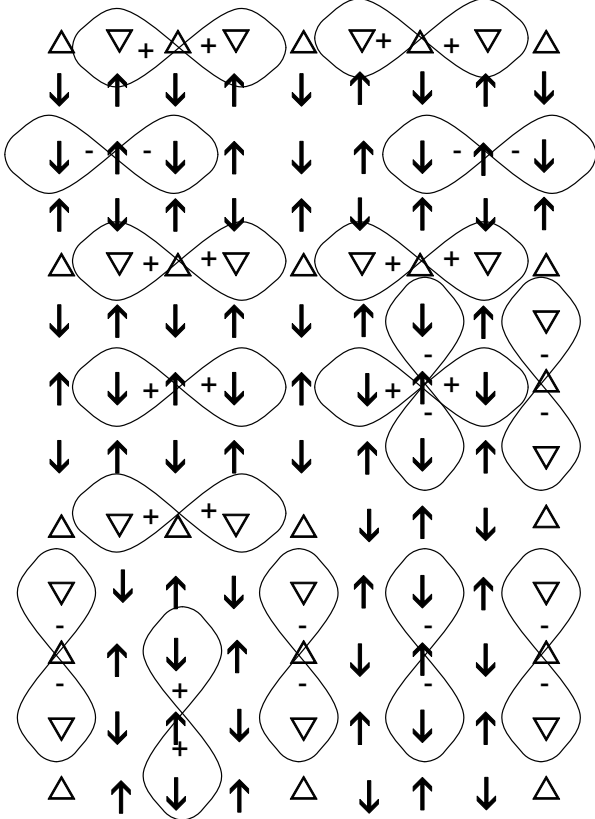


FIG. 7. An adiabatic snapshot of an extended section of a stripe-like inhomogeneity, where the available sites for the QE and stripon pairing subsets are illustrated, as well as sketches demonstrating the local symmetry of the pairing order parameters Φ^q and Φ^p .

Sketches demonstrating the local symmetry (within the adiabatic time scale) of $\Phi^q(\mathbf{r}_1, \mathbf{r}_2)$ and $\Phi^p(\mathbf{r}_1, \mathbf{r}_2)$, on the basis of Eqs. (23–26), are illustrated in Fig. 7. In these sketches point \mathbf{r}_1 is fixed on selected sites (of the \uparrow and Δ QE and stripon subsets), while point \mathbf{r}_2 is varied over the space including the nearest neighbors. Two types of local sign reversals of the order parameters are observed. One is for Φ^q on different sides of a charged stripe (serving as an anti-phase domain wall also regarding pairing). If two QE sites on different sides of a charged stripe have a stripon site midway between them, then one of them is \uparrow and the other is \downarrow , and since the exchange of the two fermion operators in the definition of Φ^q in Eq. (23) results in sign reversal, there must be sign reversal in Φ^q between the two sides. The other sign reversal is (both for Φ^q and Φ^p) between a -oriented and b -oriented stripe segments meeting in a “corner” (shown in Fig. 7). This sign reversal provides optimal pairing energy, especially in the corner regions, yielding maximal $|\Phi^q(\mathbf{r}_1, \mathbf{r}_2)|$ when \mathbf{r}_1 and \mathbf{r}_2 are at nearest neighbor QE sites [28] (where the QE’s have opposite spins and can pair), and zero $\Phi^q(\mathbf{r}_1, \mathbf{r}_2)$ when \mathbf{r}_1 and \mathbf{r}_2 are at next nearest neighbor QE sites (where the QE’s have the same spin and cannot pair).

The symmetry features of Φ^q and Φ^p , discussed above, are reflected in symmetry of the physical pairing order parameter. The overall symmetry is of $d_{x^2-y^2}$ type. However the sign reversal of Φ^q through the charged stripes, combined with the dynamics of the stripe-like inhomogeneities, and the lack of coherence between their details in different CuO_2 planes (at least in ones which are not adjacent) would result in experimental observations which are not always consistent with $d_{x^2-y^2}$ -wave pairing. The experimental conclusions concerning the gap symmetry are still somewhat controversial, though there is strong support in the existence of features of $d_{x^2-y^2}$ -wave pairing. Note that the possibility of symmetry mixtures associated with broken time-reversal symmetry (which seem to be observed experimentally) is not addressed here.

The QE and stripon pairing gaps $2\Delta^q$ and $2\Delta^p$ are closely related to Φ^q and Φ^p , and have the same symmetries. The electronic pairing gap 2Δ equals $2\Delta^q$; they vanish at the nodal points and equal $2\Delta_{\text{max}}$ at the antinodal points. Δ^p is almost constant (it is reminded that the stripon states reside around points $\pm\mathbf{k}^p$ of the lattice BZ, defined above). Δ^p is greater than Δ_{max}^q , and they are both expected to be higher when the AF/stripes effects are stronger, thus decrease with the doping level x . However the value of Δ^p is limited by the condition:

$$\Delta^p - \frac{E_{\text{res}}}{2} = \Delta^p + \bar{\epsilon}^\zeta(\mathbf{k}_0) \simeq \Delta_{\text{max}}^q = \Delta_{\text{max}}, \quad (27)$$

since above this value unpaired stripions would be formed from unpaired QE's and svivons. Thus one expects a decrease of Δ_{max} with x , scaling with the pairing temperature (T_{pair}) line in Fig. 8 (approximately according to the BCS factor [27]) as has been observed.

On the other hand, $-\bar{\epsilon}^\zeta(\mathbf{k}_0)$, which is zero for an AF, has a tendency to increase distancing from an AF state, as x rises. However, one must have:

$$\frac{E_{\text{res}}}{2} = -\bar{\epsilon}^\zeta(\mathbf{k}_0) < \Delta_{\text{max}}, \quad (28)$$

otherwise svivons around \mathbf{k}_0 would have enough energy to break pairs and, consequently, be scattered to QE-stripion states. Thus the value of $-\bar{\epsilon}^\zeta(\mathbf{k}_0)$ is expected to cross over from an increase to a decrease with x (like Δ_{max}) when their values get close to each other. And indeed, the neutron resonance energy $E_{\text{res}} = -2\bar{\epsilon}^\zeta(\mathbf{k}_0)$ has been found [20] to cross over from an increase to a decrease with x when its value gets close to $2\Delta_{\text{max}}$ (in a manner resembling the T_c line in Fig. 8).

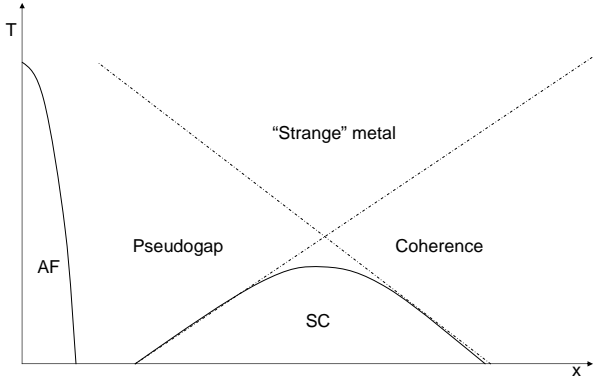


FIG. 8. A schematic phase diagram for the cuprates. The T_c line is determined by the pairing line (T_{pair}), decreasing with x , and the coherence line (T_{coh}), increasing with x (broken lines represent crossover regimes).

IX. PAIRING AND COHERENCE

The existence of SC requires not only the existence of pair correlations, but also of phase coherence of the pairing order parameters. Under conditions satisfied, for low x values, within the phase diagram of the cuprates, pairing occurs below T_{pair} , while SC occurs only below $T_{\text{coh}} (< T_{\text{pair}})$, where phase coherence sets in. The normal-state pseudogap (PG), observed in the cuprates above T_c (except for high x values) is a pair-breaking gap at

$T_{\text{coh}} < T < T_{\text{pair}}$ (see Fig. 8). Its size and symmetry are similar to those of the SC gap, and specific heat measurements [29] imply that it accounts for most of the pairing energy.

Pairing coherence requires energetical advantage of itineracy of the electronic states near E_F [8]. Thus T_{coh} is expected to increase with x (as sketched in the coherence line in Fig. 8), due to moving away from a Mott insulator, for which itineracy is energetically suppressed. This coherence argument is independent of pairing (which is energetically favorable without coherence in the PG state) and continues to be valid also in the regime of the phase diagram, shown in Fig. 8, where pairing does not exist (thus $T_{\text{coh}} > T_{\text{pair}}$). Such a determination of T_{coh} is consistent (in the regime where $T_{\text{coh}} < T_{\text{pair}}$) with a phenomenological model [30] evaluating T_{coh} on the basis of the phase “stiffness” (maintaining its coherence against fluctuations). It yields $T_{\text{coh}} \propto n_s/m_s^*$, where m_s^* and n_s are the effective pairs mass and density. This result explains the “Uemura plots” [31] in the PG doping regime (where $T_c = T_{\text{coh}}$).

Since the pair states here are fluctuating between QE and stripion pair states, the pairs density n_s is determined by the smaller of them, thus by the density of stripion pairs. The thermoelectric power results in Ref. [5] determine the occupancy of the stripion states to be 50% ($n^p = \frac{1}{2}$) for slightly overdoped cuprates ($x \simeq 0.19$). Thus the effective n_s is maximal around this stoichiometry, being determined by the density of hole-like stripion pairs for smaller x , and of particle-like stripion pairs for larger x . This explains the “boomerang-type” behavior [32] of the Uemura plots around $x \simeq 0.19$, which is a crossover regime for the value of T_c between those of T_{coh} in the underdoped regime, and of T_{pair} in the heavily overdoped regime (see Fig. 8).

Measurements of changes in the optical conductivity in the cuprates, as temperature is lowered through T_c , reveal unconventional features, which are different along the c -axis and perpendicular to it. The c -axis effects [33] below T_c are characterized, beside the opening of the SC gap, by the increase of the spectral weight at the mid-IR range (well above the gap). This effect has been observed both in bilayer and single-layer cuprates, and proposed [33] to be the signature of a c -oriented collective mode emerging (or sharpening) below T_c . Within the theory presented here of transitions between pair states of stripions and QE's, such a mode is consistent with a c -axis plasmon-type mode of such coherent pairs (below T_c). These pairs can hop in the c -direction, during their QE-pair stages, while above T_c c -axis hopping of stripions (through inter-

mediary QE–svivon states) is, at the most, limited to adjacent CuO_2 planes.

Measurements of the in-plane optical conductivity [34], as temperature is lowered through T_c , reveal, except for the overdoped regime, the transfer of spectral weight from high energies (extending over a broad range up to at least 2 eV), to the infrared range. This behavior has been associated with the establishment of coherence [35]. Within the present approach [8] it is due to the transfer of spectral weight of large- U electrons from the high-energy range, of the upper and lower Hubbard bands, to the intermediary and low energy ranges, where they participate in the formation of itinerant states based on QE’s (where hybridization with small- U electrons is included), as was worked out in Eqs. (10–18).

This coherence effect is through the coherence line in the phase diagram (see Fig. 8), and is not related to pairing. Let us regard its manifestation through the shape of ARPES peaks close to E_F , where pairing effects are not present. This is the case in nodal points (where $\Delta^q = 0$), and the effect of coherence appears to be [12] the establishment of a sharp edge to the peaks. Furthermore, in the overdoped regime coherence is expected to exist also (see Fig. 8) in a temperature range above T_c (and T_{pair}). ARPES measurements in this regime [36] show the appearance of coherence effects at $T_{\text{pair}} < T < T_{\text{coh}}$, both in nodal and antinodal peaks, consisting of the existence of a sharp peak edge and resolved bilayer-split bands.

X. PAIR-BREAKING EXCITATIONS

Both the effects of pairing and coherence are expected to exist below T_c in BZ ranges around the antinodal points. ARPES data from these ranges [37–39] as well as tunneling results [40–44], reveal a peak-dip-hump structure, appearing below T_c , but missing considerably above it in the PG regime. This structure is partly due to coherence-resolved bilayer-split bands (discussed above), but the present approach explains also another “intrinsic” aspect of this structure.

Eq. (21) distinguishes between QE and stripon-svivon contributions to the spectral structure. The linewidth of the svivon band around \mathbf{k}_0 (see Fig. 3) is expected to drop drastically below T_c , because the appearance of a coherent pairing gap (and not a partial one as in the PG regime) eliminates the scattering of these svivons to QE-stripon states. This is observed in the width of the neutron resonance peak at $E_{\text{res}} = -2\bar{\epsilon}^{\zeta}(\mathbf{k}_0)$, becoming sharp only be-

low T_c (though its remanent may be observed in the PG regime). Since the stripon bandwidth ω^p is expected [5] to be smaller than Δ^p , the stripon-svivon contribution (21) to the antinodal pair-breaking structure in the SC state [13] is expected to consist, on each side of E_F , of two peaks (and a dip between them) at distances $E_{\text{peak}} \gtrsim \Delta^p \pm \bar{\epsilon}^{\zeta}(\mathbf{k}_0)$ from E_F . By Eq. (27) the energies of these two (intrinsic) antinodal peaks can be expressed as:

$$E_{\text{peak},1} \gtrsim \Delta_{\text{max}}, \quad E_{\text{peak},2} \gtrsim \Delta_{\text{max}} + E_{\text{res}}. \quad (29)$$

Beside these two intrinsic peaks there is (21) also a QE-derived structure around the antinodal points. In bilayer cuprates it splits (below T_c) into bonding (B) and anti-bonding (AB) bands. The B band is generally not too close to the gap edge, and thus does not contribute a sharp peak, but a wide hump. On the other hand, the AB band gets very close to the gap edge (depending on x), and could, consequently, be very sharp. At different stoichiometries it may be hard to distinguish between the intrinsic peaks given in Eq. (29) and the AB peak and B hump, especially that they hybridize with each other. Tunneling results [42] on BSCCO, for different doping levels, support the result (29) of two peaks separated by E_{res} . The two peaks are also observed in ARPES results on overdoped BSCCO [38]; however the peak at $E_{\text{peak},1}$ has been identified there with that of the AB band (which for the measured stoichiometry coincides with it, and partly lies above E_F). This identification led to an analysis [45] under which there is only one intrinsic peak (at $E_{\text{peak},2}$), resulting from coupling between the B and the AB bands through the odd-symmetry neutron resonance mode. However, in recent results [39] on underdoped Pb-BSCCO, the peak at $E_{\text{peak},1}$ is identified as an intrinsic one, while that of the AB band (which for that stoichiometry lies fairly below E_F , and is thus not very sharp) is identified as “an AB hump”.

The possibility to distinguish between the intrinsic peaks (29) and QE-derived structure should be simpler in single-layer cuprates for which less “clean” experimental results exist. Tunneling results in single-layer BSCO [41] show a peak-dip-hump structure appearing below T_c , and missing in the PG state. Recent tunneling results, for different stoichiometries, in BSLCO show a hump in the PG state, splitting below T_c into two peaks, which are consistent with the intrinsic peaks given in Eq. (29). ARPES results above T_c in BSLCO [46] reveal unexpected “bilayer splitting” in the antinodal BZ area, and further measurements below T_c would be helpful to clarify whether this structure is due to the effect of the intrinsic peaks. Recent ARPES measurements on LSCO thin films [47] show that T_c rises

under strain, while the bands close to E_F become wider, and the topology of the Fermi surface around the antinodal points is altered. Further higher resolution measurements of strain effects on such films would be useful to study the antinodal excitations structure.

The spectral weight within the intrinsic peaks (29) depends on the number of stripon-svicon states within them. The svicon states are those around the minimum of $\bar{\epsilon}^\zeta$ at \mathbf{k}_0 (see Fig. 3), and thus their number approximately scales with $-\bar{\epsilon}^\zeta(\mathbf{k}_0) = E_{\text{res}}/2$, whose dependence on x [20] approximately scales with the T_c curve in Fig. 8. The stripon states are within a narrow band, which splits in the SC state [27], through the Bogoliubov transformation, into two halves (since $\omega^p < \Delta^p$), separated by $2\Delta^p$. Typical states in these upper and lower bands are created, respectively, by p_u^\dagger and p_l^\dagger . They are expressed in terms of creation and annihilation operators of stripions of the two pairing subsets (24) through equations of the form ($|u|^2 + |v|^2 = 1$):

$$p_u^\dagger = up_\Delta^\dagger + vp_\nabla^\dagger, \quad p_l^\dagger = -vp_\Delta^\dagger + up_\nabla^\dagger. \quad (30)$$

ARPES experiments at low temperatures measure the number of hole-like stripon states in the lower band, which equals $\sum |v|^2$. By BCS theory this number is $\propto (1 - n^p)$, the occupancy of the stripon states [5] in the hole representation, which approximately scales with x .

Thus, the prediction for low-temperature ARPES measurements of the x -dependence of spectral weight within the intrinsic peaks (29) is as follows: an increase with x is expected in the underdoped regime, where the number of measured states of both svicons and stripions increases with x ; on the other hand, in the overdoped regime, where the number of measured svicon states decreases with x , the increase with x of the measured spectral weight is expected to slow down, or even turn into a decrease with x . Two reports have been published [37] on such measurements in bilayer BSCCO, of the spectral weight within the peak, omitting the background (including the hump), and integrating over the antinodal BZ area. The resolution in these measurements was not sufficient to distinguish between the two peaks in Eq. (29), or to distinguish them from the AB band peak. But still they confirm the above prediction of an increase of the spectral weight with x in the underdoped regime, and its saturation, or possible turning into a decrease with x (both within the measurement error bars) in the overdoped regime. This observation support the possibility that the major contribution to the measured peak is the intrinsic one [through Eq. (29)].

XI. CONCLUSIONS

High- T_c superconductivity, and other puzzling physical properties of the cuprates, are found to result from special conditions existing for them in the regime of a Mott transition. Two features determine their phase diagram: (i) hopping-induced pairing, which depends on partial spin-charge separation, within dynamical stripe-like inhomogeneities, becomes stronger at lower doping levels, closer to the insulating side of the Mott transition; (ii) phase coherence, which is necessary for superconductivity to occur, becomes stronger at higher doping levels, closer to the metallic side of the Mott transition. A non-Fermi-liquid approach is used, treating the stripe-like inhomogeneities adiabatically. But it predicts their faster dynamics in an un-paired state, thus restoring Fermi-liquid behavior in the coherence regime.

-
- [1] J. Zaanen, and O. Gunnarsson, *Phys. Rev. B* **40**, 7391 (1989); K. Machida, *Physica C* **158**, 192 (1989); M. Kato, *et al.*, *J. Phys. Soc. Jpn* **59**, 1047 (1990); V. J. Emery, and S. A. Kivelson, *Physica C* **209**, 597 (1993).
 - [2] J. M. Tranquada *et al.*, *Phys. Rev. B* **54**, 7489, (1996); *Phys. Rev. Lett.* **78**, 338 (1997).
 - [3] O. K. Andersen *et al.*, *J. Phys. Chem. Solids* **56**, 1573 (1995).
 - [4] S. E. Barnes, *Adv. Phys.* **30**, 801 (1980).
 - [5] J. Ashkenazi, *J. Phys. Chem. Solids*, **63**, 2277-2284 (2002); cond-mat/0108383; in the High- T_c Cuprates", in *New Trends in Superconductivity*, edited by J. F. Annett and S. Kruchinin (Kluwer Academics Publishers, 2002), p. 51; cond-mat/0203170.
 - [6] J. Ashkenazi, *J. Supercond.* **7**, 719 (1994).
 - [7] The treatment of the spinons in Ref. [6] is based on an uncoupled CuO_2 plane in its basic periodicity. The existence of AF order or stripe-like inhomogeneities introduces a lower periodicity, resulting in some mixing between spinon states of different \mathbf{k} values in the lattice BZ. The existence of exchange coupling between adjacent CuO_2 planes results in a number of bare bands (as the number of coupled CuO_2 planes), the lowest of which has a V-shape zero minimum.
 - [8] The existence of QE bands, based (at least partially) on large- U states, in the vicinity of E_F requires the transfer of such states from the upper and lower Hubbard bands to this vicinity. Such a transfer occurs in the regime of a Mott transition,

- within which the cuprates are believed to be, and it is increasing with the doping level x .
- [9] J. Ashkenazi, *High-Temperature Superconductivity*, edited by S. E. Barnes, J. Ashkenazi, J. L. Cohn, and F. Zuo (AIP Conference Proceedings 483, 1999), p. 12; cond-mat/9905172.
- [10] A. Bianconi, *et al.*, *Phys. Rev. B* **54**, 12018 (1996).
- [11] H. Eskes, *et al.*, *Phys. Rev. Lett.* **67**, 1035 (1991).
- [12] T. Valla, *et al.*, *Science* **285**, 2110 (1999); A. Kaminski, *et al.*, *Phys. Rev. Lett.* **84**, 1788 (2000).
- [13] As is mentioned in the text, the stripon states are based on localized states in charged stripe-like inhomogeneities (such as shown in Fig. 7). These states are combined to yield the maximal gain in free energy due to coupling with the QE's and svivons, and combinations corresponding to areas around points $\pm\mathbf{k}^p$ in the lattice BZ are coupled optimally to high-density antinodal QE's through svivons around their minimum at \mathbf{k}_0 . The component $\frac{\pi}{2a}$ of \mathbf{k}^p perpendicular to a stripe direction is commensurate with the distance $4a$ between adjacent charged stripes. Since the charged stripes sites occupy in this case a quarter of the lattice, the areas around $\pm\mathbf{k}^p$, where stripson states reside, cover about a quarter of the lattice BZ.
- [14] T. Yoshida, *et al.*, *Phys. Rev. B* **63**, 220501 (2001).
- [15] A. Lanzara, *et al.*, *Nature* **412**, 510 (2001); X. J. Zhou, *et al.*, *Nature* **423**, 398 (2003).
- [16] P. D. Johnson, *et al.*, *Phys. Rev. Lett.* **87**, 177007 (2001).
- [17] N. P. Armitage, *et al.*, *Phys. Rev. B* **68**, 064517 (2003); cond-mat/0212172.
- [18] J. Rossat-Mignod, *et al.*, *Physica C* **185–189**, 86 (1991).
- [19] H. F. Fong, *et al.*, *Nature* **398**, 588 (1999); *Phys. Rev. B* **61**, 14773 (2000).
- [20] Ph. Bourges, *et al.*, *Science* **288**, 1234 (2000); cond-mat/0211227.
- [21] P. Dai, *et al.*, *Phys. Rev. B* **63**, 054525 (2001).
- [22] D. Reznik, *et al.*, cond-mat/0307591.
- [23] D. Reznik, *et al.*, *Phys. Rev. B* **53**, R14741 (1996).
- [24] Ph. Bourges, *et al.*, *Phys. Rev. B* **56**, R12439 (1997).
- [25] T. Yoshida, *et al.*, *Phys. Rev. Lett.* **91**, 027001 (2003).
- [26] A t -hopping of a nearest-neighbor QE pair with nearest-neighbor spin-flip (see Fig. 6) can be expressed as a combined process consisting of: (i) a transition of the QE pair into a pair state of dressed stripsons (at the same sites) by the exchange of a svivon which turns a pair of nearest-neighbor opposite spins into a singlet pair of fluctuating spins; (ii) a t -hopping of a nearest-neighbor stripon pair exchanging their sites with the sites of the nearest-neighbor fluctuating spins; (iii) a transition of the stripon pair back into a QE pair by the exchange of a svivon which turns the singlet pair of fluctuating spins into nearest-neighbor opposite spins.
- [27] The combination of Eqs. (25) and (26) results in BCS-like equations for both the QE and the stripon order parameters.
- [28] $\Phi^q(\mathbf{r}_1, \mathbf{r}_2)$ does not vanish when \mathbf{r}_1 and \mathbf{r}_2 are at nearest neighbor QE sites, both in the a and in the b directions, and has sign reversal between the two directions. Fig. 7 demonstrate this in corner regions, but it is the case also elsewhere, though there is considerable asymmetry between the a and the b directions.
- [29] C. P. Moca, and B. Jankó, *Phys. Rev. B* **65**, 052503 (2002); I. Tifrea, and C. P. Moca, cond-mat/0307362.
- [30] V. J. Emery, and S. A. Kivelson, *Nature* **374**, 4347 (1995); *Phys. Rev. Lett.* **74**, 3253 (1995); cond-mat/9710059.
- [31] Y. J. Uemura, *et al.*, *Phys. Rev. Lett.* **62**, 2317 (1989).
- [32] Ch. Niedermayer, *et al.*, *Phys. Rev. Lett.* **71**, 1764 (1993).
- [33] M. Grüninger, *et al.*, *Phys. Rev. Lett.* **84**, 1575 (2000); D. N. Basov, *Phys. Rev. B* **63**, 134514 (2001); A. B. Kuzmenko, *et al.*, *Phys. Rev. Lett.* **91**, 037004 (2003).
- [34] H. J. A. Molegraaf, *et al.*, *Science* **295**, 2239 (2002); A. F. Santander-Syro, *et al.*, *Superconducting and Related Oxides: Physics and Nanoengineering V*, edited by I. Bozovic, and D. Pavuna (SPIE Proceedings, Volume 4811, 2002), p. 48; *Europhys. Lett.* **62**, 568 (2003); cond-mat/0111539; C. C. Homes, *et al.*, *Phys. Rev. B* **69**, 024514 (2004); cond-mat/0303506.
- [35] M. R. Norman, and C. Pepin, *Phys. Rev. B* **66**, 100506 (2002); cond-mat/0302347.
- [36] Z. M. Yusof, *et al.*, *Phys. Rev. Lett.* **88**, 167006 (2002); A. Kaminski, *et al.*, *Phys. Rev. Lett.* **90**, 207003 (2003).
- [37] D. L. Feng, *et al.*, *Science* **289**, 277 (2000); H. Ding, *et al.*, *Phys. Rev. Lett.* **87**, 227001 (2001).
- [38] D. L. Feng, *et al.*, *Phys. Rev. Lett.* **86**, 5550 (2001); A. D. Gromko, *et al.*, *Phys. Rev. B* **68**, 174520 (2003); cond-mat/0202329; cond-mat/0205385.
- [39] S. V. Borisenko, *et al.*, *Phys. Rev. Lett.* **90**, 207001 (2003).
- [40] Ch. Renner, *et al.*, *Phys. Rev. Lett.* **80**, 149 (1998); M. Suzuki, and T. Watanabe, *Phys. Rev. Lett.* **85**, 4787 (2000).
- [41] M. Kugler, *et al.*, *Phys. Rev. Lett.* **86**, 4911 (2001).
- [42] J. F. Zasadzinski, *et al.*, *Phys. Rev. Lett.* **87**, 067005 (2001).
- [43] A. Yurgens, *et al.*, *Phys. Rev. Lett.* **90**, 147005 (2003).
- [44] B. W. Hoogenboom, *et al.*, *Phys. Rev. B* **67**, 224502 (2003).
- [45] M. Eschrig, and M. R. Norman, *Phys. Rev. Lett.* **89**, 277005 (2002).
- [46] C. Janowitz, *et al.*, cond-mat/0107089.

- [47] M. Abrecht, *et al.*, *Phys. Rev. Lett.* **91**, 057002 (2003).